Ultra-wideband ground penetrating radar with orbital angular momentum control

Daniel Orfeo[a], Yan Zhang[b], Dylan Burns[a], Tian Xia[b], Dryver Huston*[a]
[a]Mechanical Engineering Dept., Univ. of Vermont, 33 Colchester Ave., Burlington, VT, USA; 05405; [b]Electrical and Biomedical Engineering Dept., Univ. of Vermont, 33 Colchester Ave., Burlington, VT, USA 05405

ABSTRACT

Ultra-wideband (UWB) ground penetrating radar (GPR) is an effective, widely used tool for detection and mapping of buried targets. However, traditional ground penetrating radar systems struggle to resolve and identify congested target configurations and irregularly shaped targets. This is a significant limitation for many municipalities who seek to use GPR to locate and image underground utility pipes. This research investigates the implementation of orbital angular momentum (OAM) control in an UWB GPR, with the goal of addressing these limitations. Control of OAM is a novel technique which leverages an additional degree of freedom offered by spatially structured helical waveforms. This paper examines several free-space and buried target configurations to determine the ability of helical OAM waveforms to improve detectability and distinguishability of buried objects including those with symmetric, asymmetric, and chiral geometries. Microwave OAM can be generated using a uniform circular array (UCA) of antennas with phase delays applied according to azimuth angle. Here, a four-channel network analyzer transceiver is connected to a UCA to enable UWB capability. The characteristic phase delays of OAM waveforms are implemented synthetically via signal processing. The viability demonstrated with the method opens design and analysis degrees of freedom for penetrating radar that may help with discerning challenging targets, such as buried landmines and wires.

Keywords: Ground penetrating radar, orbital angular momentum, ultrawideband, Fractional Hilbert Transform

1. INTRODUCTION

Ground penetrating radars (GPRs) launch electromagnetic (EM) waves into earth. The waves interact with subsurface objects, layers and materials by reflecting, scattering and absorbing. The GPR receives and analyzes the return waves to render an understanding of out-of-sight subsurface features, materials and geometries. The conventional GPR uses horn or bow-tie antennas to launch waves initially as dipole radiators, often with a specified polarization, that form into spherical and eventually planar wavefronts, with nominally homogeneous properties along the wavefront. Resolving spatial dimensions relevant to GPR applications requires that the source waves contain a broad band of frequencies, i.e. are ultrawideband (UWB). Developments over the past couple decades in understanding of how EM beams, both laser and radar, propagate, and how to control the shape of the beams opens new degrees of freedom in GPR system design and operation. One of these is to control the shape of the beam, i.e., to control the 'structure' of the beam [1]. Beams with a helical structure to the waves contain orbital angular momentum (OAM) [2]. Classical descriptions of beams with OAM assume that the beam propagates with a single fixed frequency. A focus of this research is extending the operation of OAM beams to GPR by introducing UWB frequency content through synthetic methods based on superposition of single-frequency OAM beams in a manner similar to step-frequency GPR systems.

EM beams are collimated waves that propagate in a particular direction, which for GPRs is nominally vertical. Most descriptions of beams make use of the paraxial approximation. This assumes that the waves propagate as scalars, oscillate at a fixed frequency, ω, and that the angular deviation with respect to the beamline axis of the normal direction to the wavefronts are small [3]. The geometry of a paraxial beam propagating along the z-axis appears in Figure 1.

*dryver.huston@uvm.edu; phone 1 802-656-1922;

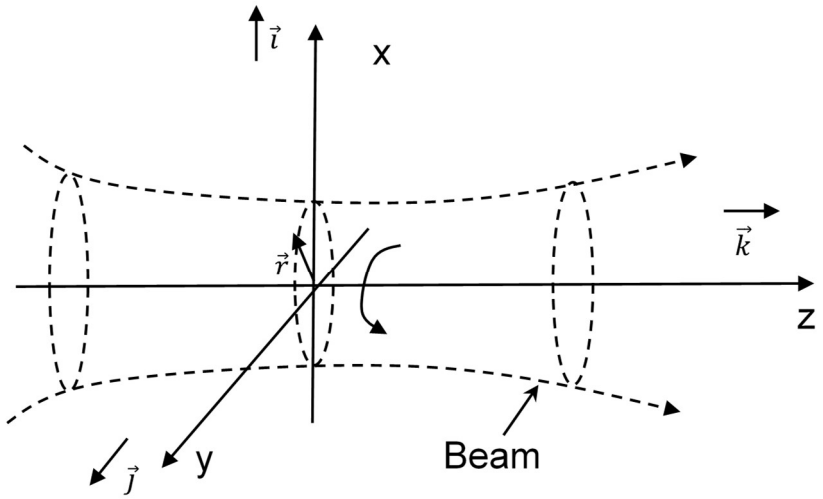

Figure 1. Electromagnetic beam centered on and propagating along z-axis with possible rotation component [2]

Since EM waves are propagating vector field disturbances, it is individual components of the electric, magnetic, or corresponding potential field that propagate as scalars. For a generic scalar, $\psi(x,y,z,t)$, the wave equation with wave speed c is

$$\nabla^2\psi = \frac{1}{c^2}\frac{\partial^2\psi}{\partial t^2} \tag{1}$$

An idealized case is when the wave oscillates at a fixed circular frequency, $\omega = 2\pi f$.

$$\psi(x,y,z,t) = \varphi(x,y,z)e^{i\omega t} \tag{2}$$

The constant frequency assumption enables reducing the wave equation into a spatial form, known as the Helmholtz equation, where $k = \omega/c$ is the circular wavenumber

$$\nabla^2\varphi + k^2\varphi = 0 \tag{3}$$

Imposing small deviation angles for the wavefront geometry with a slowly varying function A(x,y,z) creates a separable form

$$\varphi(x,y,z) = A(x,y,z)e^{-ikz} \tag{4}$$

This leads to the simple form of the paraxial wave equation

$$\frac{\partial^2 A}{\partial x^2} + \frac{\partial^2 A}{\partial y^2} - i2k\frac{\partial A}{\partial z} = 0 \tag{5}$$

Solutions to the paraxial equation give the shape of propagating beams. Multiple families of solutions exist. A simple form is if A is a constant, possibly complex. This is a plane wave propagating in the z-direction. For lasers and similar

optical beams, assuming a cylindrical paraboloidal wavefront geometry leads to the commonly cited Gaussian beam solution in cylindrical coordinates, $A_G(r, \theta, z)$ [4].

$$A_G(x, y, z) = A_1 \frac{W_0}{W(z)} \times exp\left[-\frac{r^2}{W(z)^2}\right] \times exp\left\{ik\left[z + \frac{\rho^2}{2R(z)}\right]\right\} \times \exp[i\zeta(z)] \tag{6}$$

W_0 is the beam width, z_0 is the Rayleigh range, R(z) is the wavefront curvature and $\zeta(z)$ is the Guoy phase, such that

$$W(z)^2 = W_0^2\left[1 + \left(\frac{z}{z_0}\right)^2\right] \tag{7}$$

$$R(z) = z\left[1 + \left(\frac{z}{z_0}\right)^2\right] \tag{8}$$

Other solutions to the paraxial wave equation in cylindrical coordinates exist. Of note for this research is the Gauss-LaGuerre modal solution [4]

$$A_{GLl}(r, \theta, z) = \frac{C}{\left(1+\frac{z^2}{z_R^2}\right)^{\frac{1}{2}}}\left(\frac{r\sqrt{2}}{w(z)}\right)^l L_G^l\left(\frac{2r^2}{w^2(z)}\right) \times \exp\left(\frac{-r^2}{w^2(z)}\right)\exp\left(\frac{-ikr^2z}{2(z^2+z_R^2)}\right)\exp(-il\theta) \times \exp\left(i(2p + l + 1)\operatorname{atan}\left(\frac{z}{z_R}\right)\right) \tag{9}$$

L_G^l are the Gauss-LaGuerre polynomials of integer order l. Different values of the order parameter give rise to different forms of solutions. If the order $l = 0$, the solution reverts to the Gaussian beam. If $l \neq 0$ the solution leads to helical shaped wavefronts, with the sign of l indicating the handedness of the rotation, the value of l indicating the number of intertwined helices, Figure 2. The Gauss-LaGuerre modes are mutually orthogonal when integrated over the entire 3-D space.

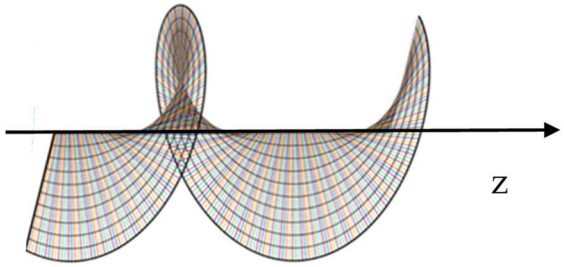

Figure 2 Wave with single helix (mode l = 1) propagating along z-axis

The Guass-LaGuerre modal solution was known as early as 1966 [4], but it did not receive much attention until 1992 where it was shown that these solutions contain waves with angular momentum and that this angular momentum directly corresponds to the angular momentum of photons [5]. There are two main types of angular momentum for photons – extrinsic and intrinsic. Extrinsic angular momentum derives from the linear angular momentum of a photon as it moves relative to a fixed axis. Intrinsic angular momentum arises from the internal action of the photon and is independent of

the choice of reference axis. Intrinsic angular momentum further separates into two components; spin angular momentum (SAM), which derives from the polarization and orbital angular momentum (OAM) corresponding to helical wavefronts around an axis corresponding to the direction of propagation [6]. EM waves propagating in free space obey superposition and may allow for conversion between SAM and OAM [7]. It is in the interaction with matter where SAM and OAM are more readily distinguished [6].

In a manner inspired by conventional radar cross sections, the OAM scattering parameter, σ_{Ol}, of an object due to a mode with helicity, l, is

$$\sigma_{Ol} \triangleq \lim_{R\to\infty} 4\pi R^2 \frac{\left|E^s_{Ol}\right|^2}{\left|E^i_{Ol}\right|^2} \tag{10}$$

$|E^s_{Ol}|^2$ and $\left|E^i_{Ol}\right|^2$ are the scattered and incident fields, respectively [8]. Determining the scattering parameter of objects largely remains an open question, with some results deriving from numerical simulations [9]. A simplistic interpretation is that if the scatterer has a helical geometry with pitch, p_s, that matches the handedness and pitch, p_i, of the incident helix, then a strong scattering signal will result. Mismatches between helicity and pitch result in smaller scattering cross-sections. The dependence of the incident wave helix pitch on frequency raises the possibility of a highly frequency and shape dependent OAM scattering cross section.

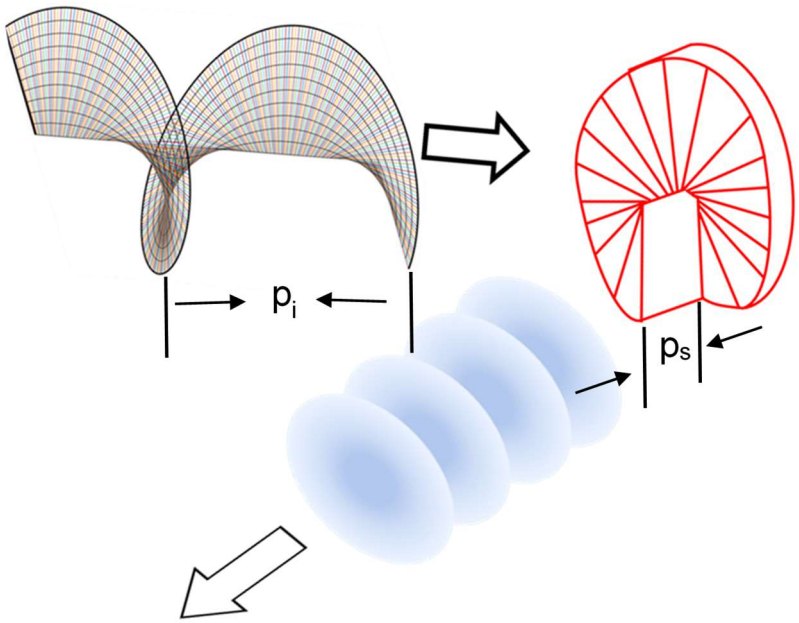

Figure 3 Match or mismatch of scattering target helical geometry with that of incident beam affects effective OAM cross-section

2. SYNTHETIC OAM

The use of OAM as a potential tool for increasing the diversity of design options and potentially improving the performance of GPRs requires effective methods of creating, receiving and processing OAM waves. One method is to launch ordinary beams with minimal OAM into a waveplate that selects and converts the incoming waves into those with OAM. Waveplate methods are effective in both the optical and microwave regimes but tend to incur large signal losses and lack flexibility in the production of different types of OAM due to the fixed solid nature of plate geometry [10] [11]. Synthetic techniques are a viable alternative to generating beams with OAM in radio and microwave frequencies [2] [8] [9]. The approach is to use a circular array of antennas to launch the waves. If the antennas broadcast at the same frequency, all that is needed is to control the phasing of the signals corresponding to the geometric phase of the antenna on the circular and the desired helicity of the outgoing wave, Figure 4.

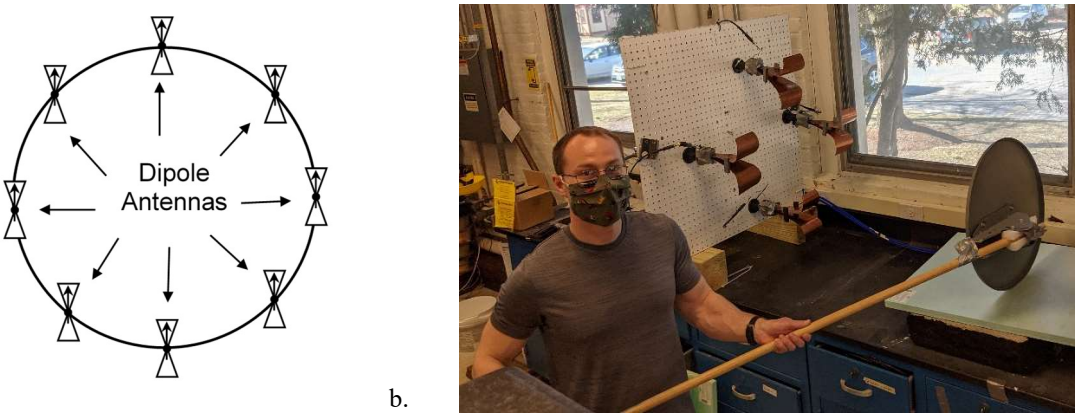

a. b.

Figure 4 Circular antenna arrays for synthetic OAM, a. schematic with array of linearly polarized dipole antennas, and b. 4-channel circular array testing scattering target with circular symmetry.

The spatial field produced by the circular array with N antennas can be represented in terms of the EM vector potential **A**(x,y,z) [13] [14], where

$$\mathbf{A}(\mathbf{r}) \sim \frac{e^{ikr}}{r} \sum_{n=1}^{N} \exp\left\{-i\left(ka\left[\cos\left(\frac{-2\pi nx}{N}\right) + \sin\left(\frac{-2\pi ny}{N}\right)\right] - \frac{2\pi nl}{N}\right)\right\} \tag{11}$$

Receiving an OAM microwave signal can make use of a circular antenna array to receive the sinusoids, at each antenna, $R_n(t)$, at the same frequency as the launch wave, and to measure the corresponding magnitude, R_n, and phase, α_n, such that

$$R_n(t) = R_n \exp[i(\omega_n t + \alpha_n)] \tag{12}$$

Inserting an OAM modal phase shift, φ_{nl}, onto each signal

$$\varphi_{nl} = \frac{2\pi nl}{N} \tag{13}$$

$$R_{nl}(t) = R_n \exp[i(\omega_n t + \alpha_n + \varphi_{nl})] \tag{14}$$

aligns the received signals in a manner that imposes OAM modal orthogonality. Combining the phase shifted signals produces the received OAM mode of interest, $R_{Ol.}(t)$

$$R_{Ol}(t) = \sum_{n=0}^{N-1} R_{nl}(t) \tag{15}$$

3. SYNTHETIC UWB GPR

GPR generally uses a broad frequency band to resolve the short spatial distances. This differs from conventional airborne and free space radars which use various forms of continuous waves with time gating to produce pulses with time of arrival indicating distance. GPRs require short pulses, on the order of 1 ns or less, to resolve the distances characteristic of subsurface feature and layer dielectric properties. Two common methods are: 1. To produce the pulses in one distinct pulse generation with circuits designed to create the impulses, such as with step recovery diodes [12]. These time-domain methods are technically challenging due to the short duration of events and large dynamic range of signals involved; and 2. Synthetic methods which use step frequency approaches. The competition between impulse and frequency domain methods predates GPR and appeared in the early days of radar and sonar developments.

Synthetic UWB steps are: 1. Select an overall UWB frequency band. 2. Pick an initial launch frequency, nominally either the upper or lower end of the UWB frequency band. 3. Launch a continuous sinusoidal EM wave into the medium under test. 4. Receive return signals at the same frequency as in step 2. 5. Measure the magnitude and phase of the return signal. 6. Increment the launch frequency by a discrete amount. Maintain the same signal amplitude or record the new launch signal amplitude. 7. Repeat steps 3 to 6 until the testing covers the entire UWB frequency band with an adequate sampling

density. 8. Convert the magnitude and phase versus frequency data of the return signals into complex number equivalents. 9. Perform an inverse discrete Fourier Transform on the return signal data to synthesize the return signal in the time domain. 10. Evaluate and manage any spurious imaginary signals in the synthesized time domain signal. Figure 5 is a diagram of the overall method. Network analyzers are standard instruments for performing synthetic impulse GPR.

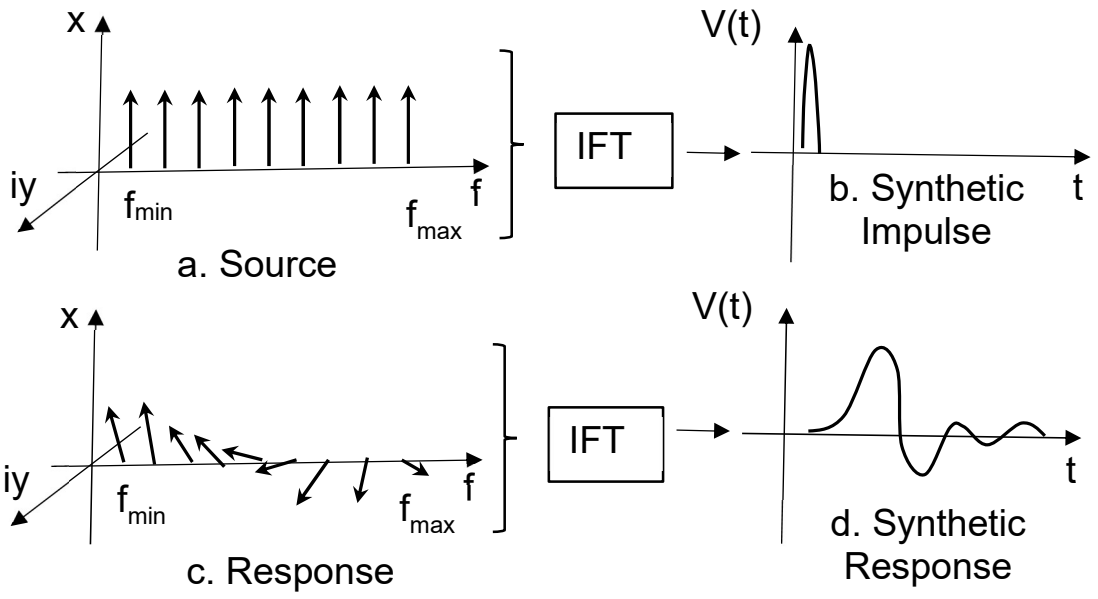

Figure 5 Operational principle of synthetic UWB GPR using step frequency method: a. Complex values of source sinusoid signals, b. Inverse Fourier Transform (IFT) converts to synthetic impulse in time domain, c. Complex values of received sinusoid signals, and d . IFT converts to synthetic impulse response in time domain

4. SYNTHETIC OAM UWB GPR

The above discussion raises the question as to whether it is possible to combine synthetic methods to extend OAM radar to the UWB regime. The overall approach is as follows: 1. Use circular array of dipole antennas operating in a phased array manner to generate helical wave at a fixed frequency with simplified phase helicity, i.e. OAM modes. 2. Collect return signals with circular array of antennas. Measure amplitude and phase at launch frequency. 3. Step launch frequency to new values. 4. Repeat steps 1 to 3 until test covers entire frequency band with sufficient sampling density. 5. Use Fractional Hilbert Transform (FHT) to decompose return signal for OAM content versus time. 6. Repeat steps 1 to 5 by using different OAM launch mode. 7. Repeat steps 1 to 6 until test covers entire range of OAM modes.

The FHT, $F_H(f)$ in step 5 introduces an OAM modal phase shift, φ_{nl} ,for each individual antenna at each frequency, f, [15].

$$H_F(f) = [\cos\varphi_{nl} + i * \mathrm{sgn}(f)\sin\varphi_{nl}][X_R(f) + i * X_I(f)] \quad (16)$$

sgn(f) is the signum function, and $X_R(f)$ and $X_I(f)$, are the real and imaginary components of the frequency domain signal amplitude components, respectively. The signum function ensures that if the original time domain function is real, the signal produced by the FHT. If the modal phase shift is $\pi/4$, then the FHT reverts to the conventional Hilbert transform.

5. EXPERIMENTS

A four-channel network analyzer (Keysight PNA-X N5241A) is the basis for a set of experiments implementing synthetic OAM GPR. The instruments collects a matrix of the magnitude and phase of the frequency response between four antennas as sources and receivers over a 0 to 13.5 GHz band, in the form of S-parameters. A first set of tests attempted to confirm whether it was possible to use OAM to measure sensitivity to helical geometries of reflectors with embedded right-hand

or left-handed helicity at a pitch in the available test frequency range. In this case targets with a sensitivity centered on 1.2 GHz were selected, Figure 6. The results of these experiments appear in Figure 7. A quick examination of the curves shows a fair amount of variation versus frequency. However, in the frequency band of interest near 1.2 GHz, the sensitivity to the particular OAM mode corresponds to that predicted from the experiments.

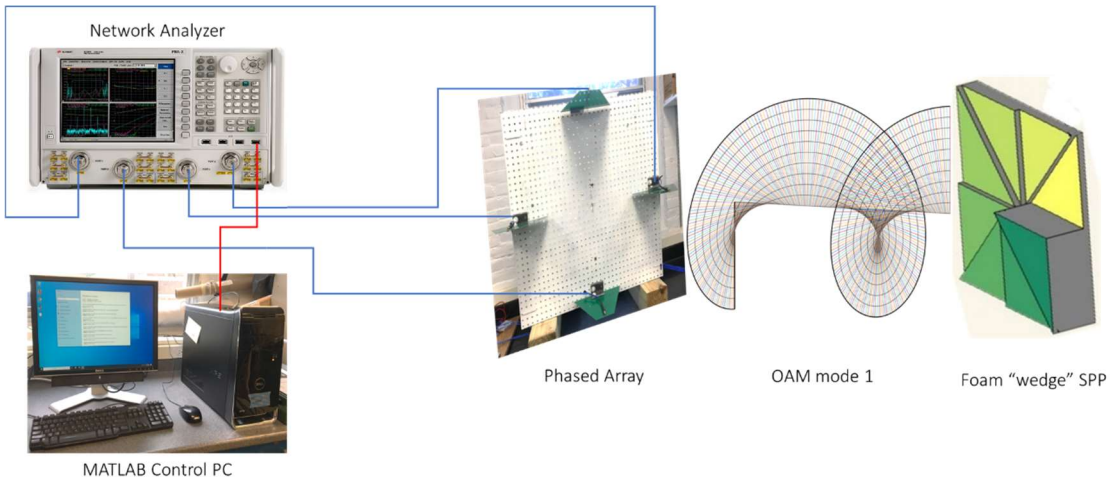

Figure 6 Experimental setup for synthetic UWB OAM GPR

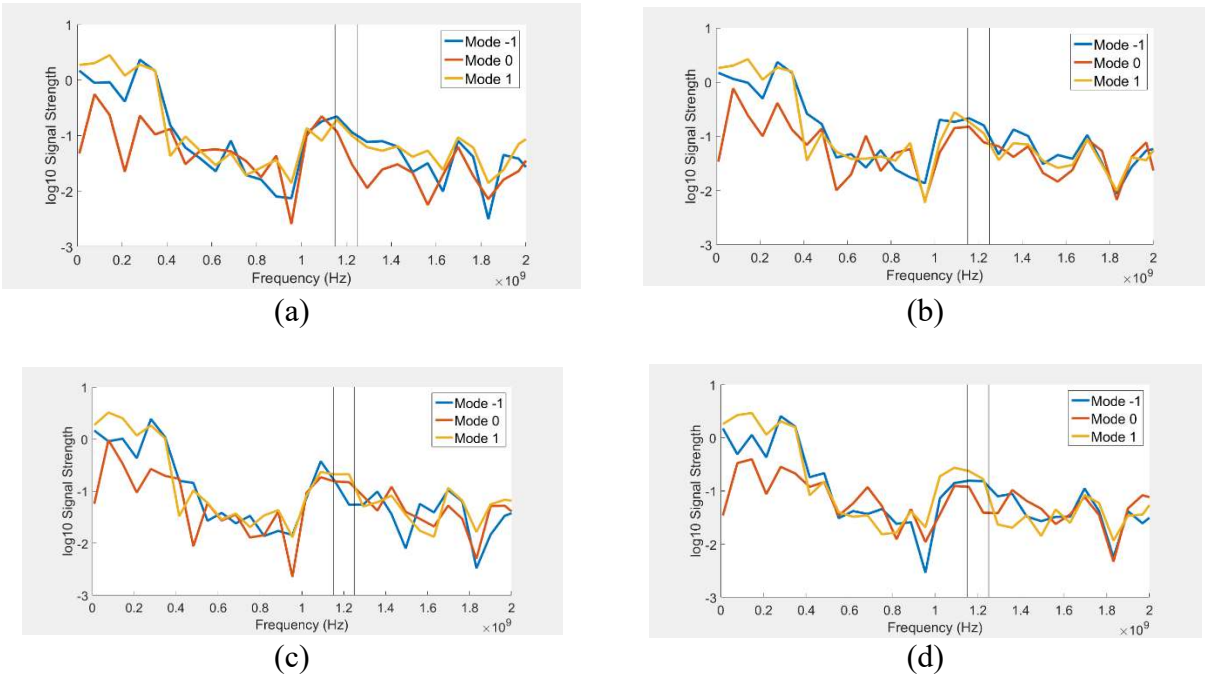

Figure 7 S11 + S22 + S33 + S44 signal magnitudes. (a) The left-handed spiral target at a 1-meter distance. Signal magnitude near 1.2 GHz is greatest when the incident signal is post-processed with OAM -1 phasing. (b) The left-handed spiral target at a 2-meter distance. Signal magnitude near 1.2 GHz is greatest when the incident signal is post-processed with OAM -1 phasing. (c) The right-handed spiral target at a 1-meter distance. Signal magnitude near 1.2 GHz is greatest when the incident signal is post-processed with OAM +1 phasing. (d) The right-handed spiral target at a 2-meter distance. Signal magnitude near 1.2 GHz is greatest when the incident signal is post-processed with OAM +1 phasing.

Next a series of measurements were conducted with the synthetic OAM UWB GPR system on various additional shapes. A circular TV dish antenna served as a strong reflector with cylindrical symmetry, Figure 4. A strong smooth set of scattering curves formed when the antenna was centered on the circular antenna array axis. The reflection curves changed with the position of the antenna to off-axis configurations. The scattering from various geometries of wire bundles appears in Figure 9 to Figure 11. In all of these cases the scattering curves changed significantly with changes in geometry.

a. 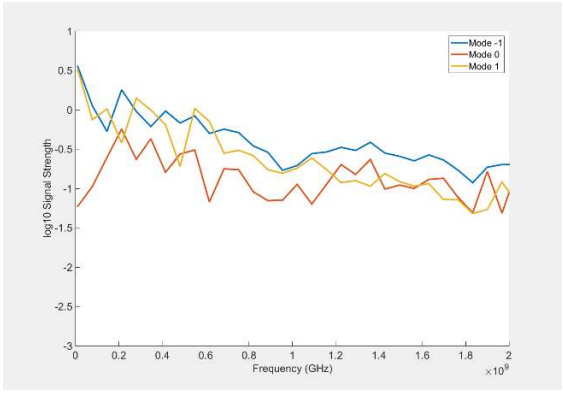

b. 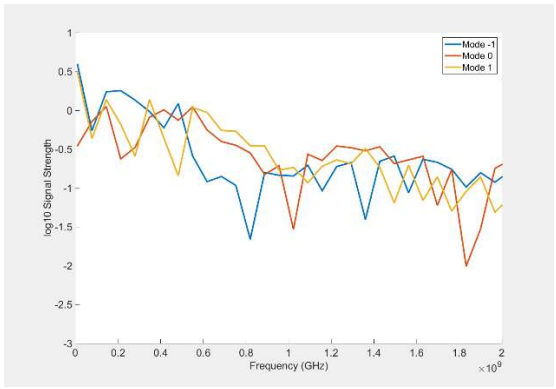

Figure 8 Scattering of OAM modes from circular TV dish antenna; a. Centered on antenna array axis, and b. Offset 0.3 m from antenna array axis.

a. 
b. 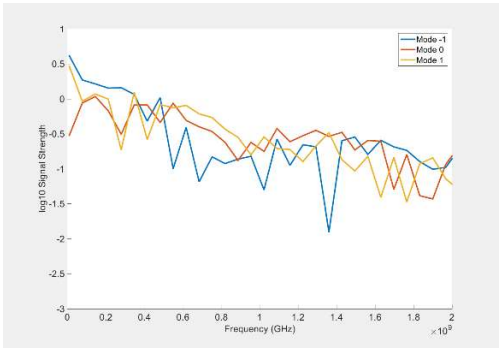

Figure 9 Scattering of OAM modes from a circular wrapped wire bundle

a. 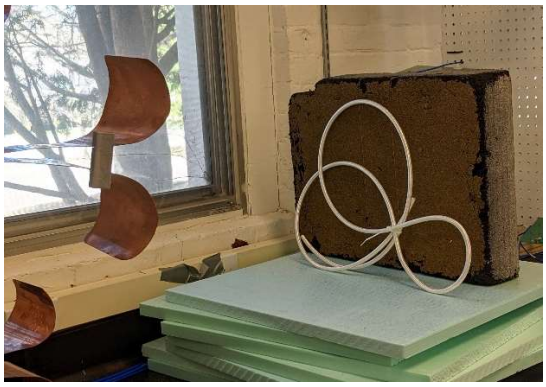
b. 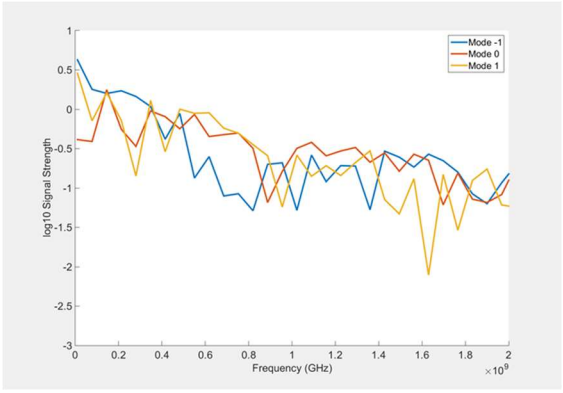

Figure 10 Scattering of OAM modes from a pretzel-shaped wire bundle

a.  b. 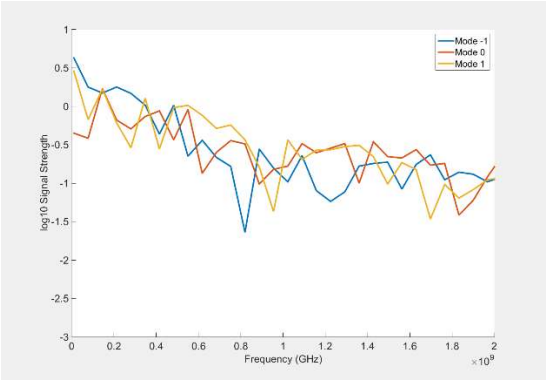

Figure 11 Scattering of OAM modes from an ell-shaped wire bundle

6. CONCLUSIONS

Control of the shape, i.e., structure, introduces additional degrees of freedom for the design of penetrating radar systems. Beams with OAM have the potential to interact with material objects in manners that differs from non-OAM beams. Conventional implementations of OAM use a single fixed frequency. GPRs require operation with wide, even ultra-wide frequency bands. Synthetic methods can extent OAM to UWB frequency bands with potential for use in GPR. Experiments with synthetic OAM UWB radar using a four-channel network analyzer confirm sensitivity to helical geometry as predicted, and sensitivity to geometry and position of various scattering objects, including those with circular symmetry and wire bundles. Many issues regarding understanding OAM modal scattering parameters from various objects remain open for further investigation. Since EM beams superpose in free space, there may be other favorable array arrangements for penetrating radars as well.

7. ACKNOWLEDGEMENTS

This work has been supported by Defense University Research Instrumentation Program (DURIP) U.S. Army contract no. W911NF1810193, U.S. Army contract W909MY-17-C-0020 with White River Technologies, Inc., U.S. National Science Foundation grants 1647095 and 1640687, University of Vermont SPARK Fund, University of Vermont Office for the Vice President for Research, and the Vermont Space Grant Consortium under NASA Cooperative Agreement NNX15AP86H.

REFERENCES

[1] Yao, A. M. and Padgett, M. J., “Orbital angular momentum: origins, behavior and applications” Adv. Opt. Photon., 3(2):161-204 (2011).
[2] Orfeo, D., Ezequelle, W., Xia, T., Huston, D. R., “Orbital Angular Momentum Assisted Ground Penetrating Radar” Proc. SPIE, 11012-47 (2019)
[3] Saleh, B. E., Teich, M. E., [Fundamental of Photonics], Wiley, New York, 45-51 (1991).
[4] Kogelnik H., Li T., “Laser Beams and Resonators,” Applied Optics 5(10), 1550-1567 (1966).
[5] Allen, L., Beijersbergen, M.W., Spreeuw, R.J., and Woerdman, J.P., “Orbital Angular Momentum of Light and the Transformation of Laguerre-Gaussian Laser Modes” Phys. Rev. A 45, 8185 (1992).
[6] Bliokh, K.Y., Nori, F., “Transverse and longitudinal angular momenta of light” Physics Reports, 592, 1-38 (2015).
[7] Feynman, R. P., Leighton, R. B., Sands, M., [Mainly Electromagnetism and Matter. The Feynman Lectures on Physics. Vol. 2.] Addison-Wesley, Reading, MA, 20-8 (1964).
[8] Liu, K., Gao, Y., Li, X., Cheng, Y., “Target scattering characteristics for OAM-based radar” AIP Advances 8, 025002 (2018)
[9] Orfeo D. J., Burns D., Huston D. R., Xia T., “Wideband Synthetic Orbital Angular Momentum Radar” Journal of Applied Remote Sensing, J. 15(1), 017504, (2021)
[10] Pu, M., Li, X., Ma, X., Wang, Y., Zhao, Z., Wang, C., Hu, C., Gao, P., Huang, C., Ren, H., Li, X., Qin, F., Yang, J., Gu, M., Hong, M., and Luo X., “Catenary Optics for Achromatic Generation of Perfect Optical Angular Momentum,” Science Advances, 1, 9, e1500396 (2015).

[11] Cheng, L., Hong, W., and Hao, Z. C., “Generation of Electromagnetic Waves with Arbitrary Orbital Angular Momentum Modes” Scientific Reports 4, Article number: 4814 (2014).
[12] Xia T., Venkatachalam A. B., Huston D., “A high performance low ringing ultra-wideband monocycle pulse generator” IEEE Transactions on Instrumentation and Measurement, 61(1), 261 - 266 (2012)
[13] Mohammadi, S.M., Daldorff, L.K., Bergman, J.E., Karlsson, R.L., Thide, B., Forozesh, K., Carozzi, T.D., and Isham, B., “Orbital angular momentum in radio- a system study” IEEE Transactions on Antennas and Propagation, 58(2), 565-572 (2010)
[14] Liu, K., Cheng, Y., Yang, Z., Wang, H., Qin, Y., and Li, X., “Orbital-angular-momentum-based electromagnetic vortex imaging” IEEE Antennas and Wireless Propagation Letters, 14, 711-714 (2015)
[15] Lohmann, A.W., Mendlovic, D., Zalevsky, Z., “Fractional Hilbert transform” Optics Letters, 21(4), 281-283 (1996).